

# Wavemaker theories for acoustic-gravity waves over a finite depth

Miao Tian<sup>1,2</sup>, Usama Kadri<sup>3,4</sup>

1. Department of Physical Oceanography, Woods Hole Oceanographic Institute, Woods Hole, MA 02543, USA.
2. The Hatter Department of Marine Technologies, University of Haifa, Haifa 3498838.
3. School of Mathematics, Cardiff University, Cardiff, CF24 4AG, UK.
4. Department of Mathematics, Massachusetts Institute of Technology, Cambridge, MA 02139, USA.

## Abstract

Acoustic-gravity waves (hereafter AGWs) in ocean have received much interest recently, mainly with respect to early detection of tsunamis as they travel at near the speed of sound in water which makes them ideal candidates for early detection of tsunamis. While the generation mechanisms of AGWs have been studied from the perspective of vertical oscillations of seafloor and triad wave-wave interaction, in the current study we are interested in their generation by wave-structure interaction with possible implication to the energy sector. Here, we develop two wavemaker theories to analyze different wave modes generated by impermeable (the classic Havelock's theory) and porous (porous wavemaker theory) plates in weakly compressible fluids. Slight modification has been made to the porous theory so that, unlike the previous theory, the new solution depends on the geometry of the plate. The expressions for three different types of plates (piston, flap, delta-function) are introduced. Analytical solutions are also derived for the potential amplitude of the gravity, acoustic-gravity, evanescent waves, as well as the surface elevation, velocity distribution, and pressure for AGWs. Both theories reduce to previous results for incompressible flow when the compressibility is neglected. We also show numerical examples for AGWs generated in a wave flume as well as in deep ocean. Our current study sets the theoretical background towards remote sensing by AGWs, for optimized deep ocean wave-power harnessing, among others.

## 1 Introduction

Wavemaker theory has received increasing attention not only because its feasibility on generating waves in laboratory experiments, but also due to its application in design of wave-energy harnessing devices (Mei, 2012). The classic problem of surface waves generated by a wavemaker in

infinitely deep ocean was investigated by Havelock, as in Ref. Havelock (1929), and later extended to the case of finite water depth (e.g., Ursell et al., 1960). The wavemaker was treated as a vertical impermeable plate which oscillates horizontally and periodically with a small displacement, and the fluid was assumed incompressible. In all these formulations the wave motion was governed by linear wave theory. Extensions to a directional wavemaker problem with slowly-varying depth can be found in Dalrymple (1989).

The impermeability of the plate is unrealistic for a plate in a wave flume, not to mention a landslide in deep ocean. Madsen (1970) examined the influence of leakage around the wavemaker on the wave amplitude and concluded that the porous effect can largely reduce the wave amplitude. Therefore it would be more appropriate to take porosity effects into account for many applications.

Recently, acoustic-gravity waves (hereafter AGWs) in a compressible ocean have received much interest, because AGWs travel significantly faster than the tsunami, and become ideal candidates for early detection of tsunami by the use of bottom-pressure records (Stiassnie, 2010; Hendi and Stiassnie, 2013). AGWs can interact with continental shelves (Kadri and Stiassnie, 2012), ice-sheets (Kadri, 2016b), and bluemight be responsible for deep-ocean bluewater transportation and circulation (Kadri, 2014). In contrast to the decaying vertical structure of gravity-wave modes, the wave amplitudes of AGWs exhibit sinusoidal variation in the vertical direction. Therefore wave-energy harnessing devices that are placed in deep water (where the decaying gravity wave modes vanish) can potentially make use of AGWs, because the induced measurable pressure signature may reach a maximum at the seabed. While harnessing energy of AGWs might become possible in the future, e.g. based on a triad interaction mechanism similar to that presented by Kadri (2016a) or Kadri and Akylas (2016), a more immediate application is the detection of sea-state in wave harnessing farms. Here, we show that AGWs radiate by the harnessing devices, or namely wave-makers, carrying information on their source at the speed of sound in water. To this end, while the generation mechanisms of AGWs have been studied from the perspective of vertical oscillations of seafloor (Yamamoto, 1982; Stiassnie, 2010; Oliveira and Kadri, 2016) and triad wave-wave interaction (Kadri and Stiassnie, 2013; Kadri, 2015, 2016a; Kadri and Akylas, 2016), here we are particularly interested in their generation by horizontally-moving wavemakers.

We develop Havelock's and porous wavemaker theories for weakly compressible fluids. The paper is organized as follows: in section 2 the problem is formulated with the governing equations, while the wavemakers is treated as along-channel boundary conditions. The general solution to the governing equations is presented in Section 3, followed by the Havelock's and porous-wavemaker solutions in Section 4. Section 5 presents examples for three types of wavemaker placed in a wave flume as well as in deep ocean. The work is summarized in Section 6.

## 2 Governing equations

We take  $x$  and  $z$  the horizontal and cal coordinate respectively, and consider a wavemaker with its plate initially located at  $x = 0$ . The wavemaker oscillates horizontally along the  $x$ -axis with a displacement  $s_0$  given by

$$s_0(x, z, t) = d(z) \exp(-i\omega t), \quad d \ll h \quad (1)$$

where  $\omega$  is the radian frequency,  $d(z)$  is the maximum amplitude of oscillation, assumed to be much smaller than the undisturbed fluid depth  $h$ , and  $t$  is the time. The horizontal velocity and acceleration of the wavemaker are

$$u_0 = -i\omega d \exp(-i\omega t), \quad a_0 = -\omega^2 d \exp(-i\omega t). \quad (2)$$

The equation that governs the irrotational motions of acoustic-gravity waves throughout the entire water column is

$$\Phi_{tt} = c^2 (\Phi_{xx} + \Phi_{zz}), \quad -h < z < \eta, \quad (3)$$

where  $\Phi$  is the velocity potential, and  $c$  is the speed of sound in water. The linearized kinematic and dynamic conditions at the free surface are

$$\Phi_z = \eta_t, \quad z = \eta, \quad (4)$$

$$\Phi_t + g\eta = 0, \quad z = \eta, \quad (5)$$

where  $\eta$  is the free surface elevation. Expanding (4) and (5) at  $z = 0$  and eliminating  $\eta$  yield the approximated surface boundary condition (e.g., Lamb 1916)

$$\Phi_{tt} + g\Phi_z = 0, \quad z = 0. \quad (6)$$

Finally the kinematic bottom boundary condition for a flat bottom is given by

$$\Phi_z = 0, \quad z = -h, \quad (7)$$

which indicates the vertical velocity of the fluid must be zero at the bottom.

Equations (3), (6), and (7) formulate the linear problem of water wave propagation over a finite depth in a weakly compressible fluid. Appropriate along-channel boundary conditions depending on the types of wavemaker can be included to define the problem completely.

For the classic Havelock's wave-maker theory (e.g., Havelock, 1929; Ursell et al., 1960; Stuhlmeier and Stiassnie, 2015), the boundary condition is

$$\Phi_x = u_0, \quad x = 0 \quad (8)$$

where  $u_0$  is the horizontal velocity of the stroke motion.

For a porous-wavemaker problem, the boundary condition at the wavemaker is given by Chwang Chwang (1983). The hydrodynamic pressure  $p(x, z, t)$  is associated with the velocity potential  $\Phi$  via the linearized Bernoulli equation as

$$p = -\rho\Phi_t \quad (9)$$

in which  $\rho$  is the water density.

The pressure on the positive and negative sides of the wavemaker are related as

$$p(0, z, t) = p^+(z, t) = -p^-(z, t). \quad (10)$$

The normal velocity towards the porous plate is equal to the velocity of the stroke motion  $u_0$ , which is linearly proportional to the pressure difference between the two sides of the wavemaker (Taylor, 1956), so that

$$u_0(z, t) = \frac{2b}{\mu} p(0, z, t) \quad (11)$$

Here,  $\mu$  is the dynamic viscosity, and  $b$  is the coefficient which represents the width of the plate and has the dimension of a length.

### 3 General Solution

In accordance with the periodic motion of the wavemaker,  $\Phi$ ,  $\eta$ , and  $p$  are assumed to be periodic functions in  $t$  with a time factor  $\exp(-i\omega t)$ , i.e.

$$\Phi = \phi(x, z) \exp(-i\omega t), \quad \eta = a(x) \exp(-i\omega t), \quad p = p(x, z) \exp(-i\omega t). \quad (12)$$

Using (12), equation (3) reduces to

$$\phi_{xx} + \phi_{zz} + k_c^2 \phi = 0, \quad k_c = \omega/c, \quad (13)$$

where  $k_c$  is a compressibility coefficient. Similarly, substituting equation (12) into equations (6) and (7) yields the boundary conditions in terms of  $\phi$ ,

$$-\omega^2 \phi + g\phi_z = 0, \quad z = 0; \quad (14)$$

$$\phi_z = 0, \quad z = -h. \quad (15)$$

Following similar steps as in Stiassnie (2010) and Yamamoto (1982) the solution of equations (13)-(15) is obtained,

$$\begin{aligned} \phi = & A_0 \exp(ik_0 x) \cosh(\lambda_0(z+h)) \\ & + \sum_{n=1}^N A_n \exp(ik_n x) \cos(\lambda_n(z+h)) \\ & + \sum_{n=N+1}^{\infty} B_n \exp(-\kappa_n x) \cos(\lambda_n(z+h)), \end{aligned} \quad (16)$$

Here,  $\lambda_0$  and  $\lambda_n$  (real and positive) are the solutions of

$$\omega^2 = g\lambda_0 \tanh(\lambda_0 h); \quad (17)$$

$$\omega^2 = -g\lambda_n \tan(\lambda_n h), \quad n = 1, 2, 3, \dots, \quad (18)$$

where  $\lambda_n$  is the  $n$ -th eigenvalue and  $n$  is the mode number. With specified  $\omega$  and  $h$ , equation (17) has one real solution for  $\lambda_0$ ; while equation (18) involves infinitely-many different  $\lambda_n$ .

Here,  $k_0$ ,  $k_n$ ,  $\kappa_n$  (real and positive) are given by

$$k_0 = \sqrt{k_c^2 + \lambda_0^2}, \quad (19)$$

$$k_n = \sqrt{k_c^2 - \lambda_n^2}, \quad n = 1, 2, \dots, N; \quad k_c > \lambda_N, \quad (20)$$

$$\kappa_n = \sqrt{\lambda_n^2 - k_c^2}, \quad n = N+1, \dots; \quad k_c < \lambda_{N+1} \quad (21)$$

where  $N$  represents the nearest integer smaller than  $[\frac{\omega h}{\pi c} + \frac{1}{2}]$ , as in Ref. (Kadri and Stiassnie, 2012). The three terms on the right-hand-side of equation (16) represent the gravity, acoustic-gravity, and evanescent modes, respectively.

## 4 Wavemaker problem

### 4.1 Solution for Havelock's wavemaker

Since  $\cosh(\lambda_0(z+h))$  and  $\cos(\lambda_n(z+h))$  in equation (16) are the eigenfunctions of the boundary value problem in  $z$ , they are orthogonal over the interval from  $z = 0$  to  $z = -h$  based on the Sturm-Liouville theory. Therefore we substitute equations (12), and (16) into equation (8), multiply by  $\cosh(\lambda_0(z+h))$  and  $\cos(\lambda_n(z+h))$  and integrate over the water column from  $z = -h$  to  $z = 0$  so that  $A_0, A_n, B_n$  can be calculated as

$$A_0 = \frac{-2\omega}{h\sqrt{k_c^2 + \lambda_0^2}(1 + CQ_0^2)} \int_{-h}^0 d \cosh(\lambda_0(z+h)) dz, \quad (22)$$

$$A_n = \frac{-2\omega}{h\sqrt{k_c^2 - \lambda_n^2}(1 - CQ_n^2)} \int_{-h}^0 d \cos(\lambda_n(z+h)) dz, \quad (23)$$

$$B_n = \frac{2i\omega}{h\sqrt{\lambda_n^2 - k_c^2}(1 - CQ_n^2)} \int_{-h}^0 d \cos(\lambda_n(z+h)) dz, \quad (24)$$

where

$$Q_0 = \sinh \lambda_0 h, \quad Q_n = \sin \lambda_n h, \quad C = \frac{g}{\omega^2 h}. \quad (25)$$

In the incompressible case ( $c \rightarrow \infty$ ), equations (22) and (24) are essentially the same as the solutions for gravity and evanescence modes in Dean and Dalrymple (1991) (equations (6.21) and (6.22)). The extra term  $A_n$  comes from the newly-generated AGW mode due to the compressibility of the fluid.

### 4.2 Solution for porous wavemaker

Following similar steps using (11) together with (9), (12), and (16) and the orthogonality of  $\cosh(\lambda_0(z+h))$  and  $\cos(\lambda_n(z+h))$ , we can derive expressions of  $A_0, A_n, B_n$  for a porous wavemaker. Chwang (1983) described a similar problem for incompressible flow and derived the solutions. Chwang's solution, however, indicates that the produced waves have the same amplitudes regardless of the geometry of the plate. In order to consider different plate types, we modified Chwang's method and derive an alternative solution in a similar form as the Havelock's

(Dean and Dalrymple, 1991)

$$A_0 = G_0 \frac{-2\omega}{h\sqrt{k_c^2 + \lambda_0^2} (1 + CQ_0^2)} \int_{-h}^0 d \cosh(\lambda_0(z+h)) dz, \quad (26)$$

$$A_n = G_n \frac{-2\omega}{h\sqrt{k_c^2 - \lambda_n^2} (1 - CQ_n^2)} \int_{-h}^0 d \cos(\lambda_n(z+h)) dz, \quad (27)$$

$$B_n = H_n \frac{2i\omega}{h\sqrt{\lambda_n^2 - k_c^2} (1 - CQ_n^2)} \int_{-h}^0 d \cos(\lambda_n(z+h)) dz, \quad (28)$$

where the porous factors are

$$G_0 = \frac{\mu\sqrt{k_c^2 + \lambda_0^2}}{2\omega\rho b}, \quad G_n = \frac{\mu\sqrt{k_c^2 - \lambda_n^2}}{2\omega\rho b}, \quad n = 1, 2, \dots, N, \quad (29)$$

$$H_n = \frac{-i\mu\sqrt{\lambda_n^2 - k_c^2}}{2\omega\rho b} \quad n = N+1, N+2, \dots$$

We focus on the porous factor  $G_n$  that is associated with AGW modes. As pointed out in Chwang (1983), the reciprocal of  $G_n$  in equation (29) can be understood as a Reynolds number for the flow passing through the porous wavemaker, while  $G_n$  also measures the porosity. For example,  $G_n = 0$  (or equivalently,  $\mu = 0$ ) means the wavemaker is completely permeable. Obviously, the expressions reduce to the Havelock's solution when the porous factors,  $G_0$ ,  $G_n$ ,  $H_n$ , are unity. Moreover, as  $\lambda_n$  increases with mode number  $n$ , the porous factor  $G_n$  decreases for higher AGW modes, meaning that the porous media dissipates more energy from shorter waves (lower modes). Specifying values for the porous factor of the gravity mode  $G_0$  (0.1, 0.2, 0.5, etc.), Chwang (1983) showed surface elevation of gravity waves produced by the wavemaker. In this study, the porous factor for the first AGW mode  $G_1$  will be set to 0.5 for illustration purposes, while  $G_n$  ( $n = 2, 3, \dots$ ) can be determined based on that.

The amplitudes of the surface elevation, horizontal velocity, and pressure at AGW mode  $n$  can also be given employing equations (5), (9), (12), (16)

$$a_n = i\frac{\omega}{g}A_n \exp\left(i\sqrt{k_c^2 - \lambda_n^2}x\right) \cos(\lambda_n h); \quad (30)$$

$$u_n = i\sqrt{k_c^2 - \lambda_n^2}A_n \exp\left(i\sqrt{k_c^2 - \lambda_n^2}x\right) \cos(\lambda_n(z+h)); \quad (31)$$

$$p_n = i\omega\rho A_n \exp\left(i\sqrt{k_c^2 - \lambda_n^2}x\right) \cos(\lambda_n(z+h)); \quad (32)$$

where  $A_n$  is defined in equation (27).

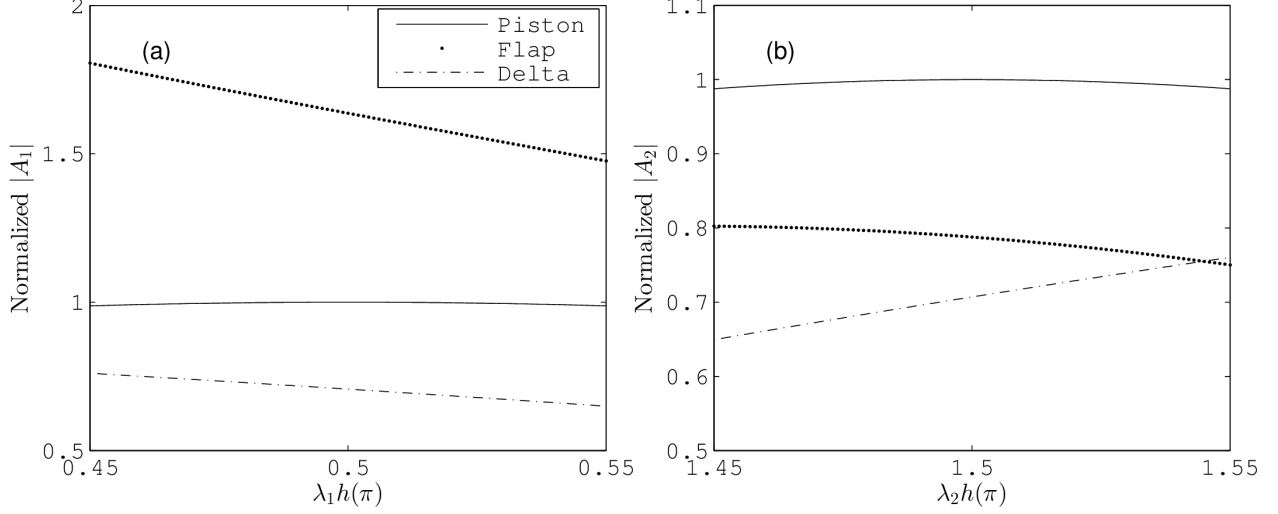


Figure 1: Normalized AGW velocity potential amplitudes  $|A_1|$  (a) and  $|A_2|$  (b) by a factor of  $-2\omega D/\lambda_n h \sqrt{k_c^2 - \lambda_n^2} (1 - CQ_n^2)$  ( $n = 1$  and  $2$ , respectively) for three types of plate as a function of  $\lambda_n h$ , which is chosen to vary between  $[0.45, 0.55]n\pi$ . The  $\delta$ -function type wavemaker is assumed to be located at  $z = -h/2$  for illustration purposes. Solid: piston-type plate; dotted: flap-type plate; dashed:  $\delta$ -function type plate.

### 4.3 Different types of plates

We focus on the AGWs term in equations (23) and (27) and derive the explicit form based on different types of the plate. Piston and flap motions (Dean and Dalrymple, 1991) are commonly used for wave flumes in laboratory experiments, while a wavemaker of  $\delta$ -function type is considered for deep ocean (Stuhlmeier and Stiassnie, 2015). Therefore the function  $d(z)$  that describes the piston motion in equation (1) has been assumed to be

$$d(z) = \begin{cases} D, & \text{piston plate;} \\ D(1 + z/h), & \text{flap plate;} \\ D\delta(z + h_0), & \delta\text{-function plate.} \end{cases} \quad (33)$$

Here,  $D$  is the horizontal amplitude of the stroke motion. The  $\delta$ -function type wavemaker is located at  $z = -h_0$ .

Substituting equation (33) into the Havelock's solution (23), the expression for the amplitude of the velocity potential,  $A_n$ , can be readily obtained

$$A_n = \begin{cases} \frac{-2\omega D}{\lambda_n h \sqrt{k_c^2 - \lambda_n^2} (1 - CQ_n^2)} \sin(\lambda_n h), & \text{piston plate;} \\ \frac{-2\omega D}{\lambda_n h \sqrt{k_c^2 - \lambda_n^2} (1 - CQ_n^2)} \frac{1}{\lambda_n h} [\lambda_n h \sin(\lambda_n h) + \cos(\lambda_n h) - 1], & \text{flap plate;} \\ \frac{-2\omega D}{\lambda_n h \sqrt{k_c^2 - \lambda_n^2} (1 - CQ_n^2)} \cos(\lambda_n (h - h_0)), & \delta\text{-function plate.} \end{cases} \quad (34)$$

A comparison of the normalized velocity potential amplitude in equation (34) is given in Figure 1. Apparently, a flap wavemaker produces the largest first-mode AGW for the same plate-motion



amplitude  $D$ . For a flap plate, equation (34) also indicates that the normalized AGW amplitudes are inversely proportional to  $\lambda_n h$ , therefore higher AGW modes must have smaller normalized amplitudes.

## 5 Examples

### 5.1 Acoustic-gravity waves in a wave flume

The number of existing AGW modes associated with specific frequency and depth can be calculated by equation (17). This relationship shows that more AGW modes can be generated at a higher frequency  $\omega$  or deeper water. Therefore, creating AGWs in the laboratory is not an easy task. In order to obey AGW theory (with the absence of bottom elasticity, e.g. see Eyov et al. (2013) for the detailed analysis) and create AGWs in the laboratory experiments we need to operate at relatively very high frequencies. For example, there are three AGW modes corresponding to a 5 kHz wavemaker in a 0.5 m wave flume. Although, working with a 5 kHz introduces some real difficulties, we can still have feasible experiments with piezoelectric membranes to validate the proposed theory (an undergoing research). Alternatively, one needs to carry out an experiment in the deep ocean, which is by no means easier to perform. Due to this conflicting choice of experimental environment, we dedicate this section and the following to the disparate wave flume and deep ocean systems, respectively.

Examples of AGWs generated in a wave flume by piston- and flap-type plates are shown in Figures 2 and 3 based on Havelock's and porous wavemaker theories, respectively. Notice that the stroke motion is not only limited by its maximum stroke distance, but also the maximum velocity and acceleration. Here, we assume the wavemaker has the same constraints as the unidirectional wavemaker of the O.H. Hinsdale Wave Research Laboratory in Oregon State University (for example the laboratory experiment presented in Tian et al., 2015); simple calculation using equations (2) shows that the stroke amplitude of a wavemaker with  $f = 5$  kHz is at the order of  $10^{-8}$  m, which requires a very careful experiment.

It is difficult to measure the AGWs surface elevations directly because of their small amplitudes (not shown in the figure), although the horizontal velocity component is at the order of  $10^{-3}$  m/s (Figure 2 (a) and (c)), which is detectable using a particle image velocimetry (PIV) system. It is also worth mentioning that, unlike gravity waves, AGWs velocity amplitude oscillates vertically and leaves a distinct pressure signature throughout the entire water column, and in particular at the bottom.

The time series of the pressure at the bottom (Figure 2 (b) and (d)) behaves similarly as that of the surface elevation, although measurable by a wired pressure sensor. Therefore, in spite of the small amplitude of their surface elevation, AGWs are expected to be detectable on bottom-pressure records or PIV velocity measurement in a laboratory study. On the other hand the flap wavemaker is able to produce larger waves compared to a piston one as shown in Figure 2 (c) and (d). Figure 3 presents AGWs-induced pressure and velocities produced by porous wavemakers. Due to porosity effects, the velocity and pressure amplitudes are generally smaller than these in Havelock's theory.



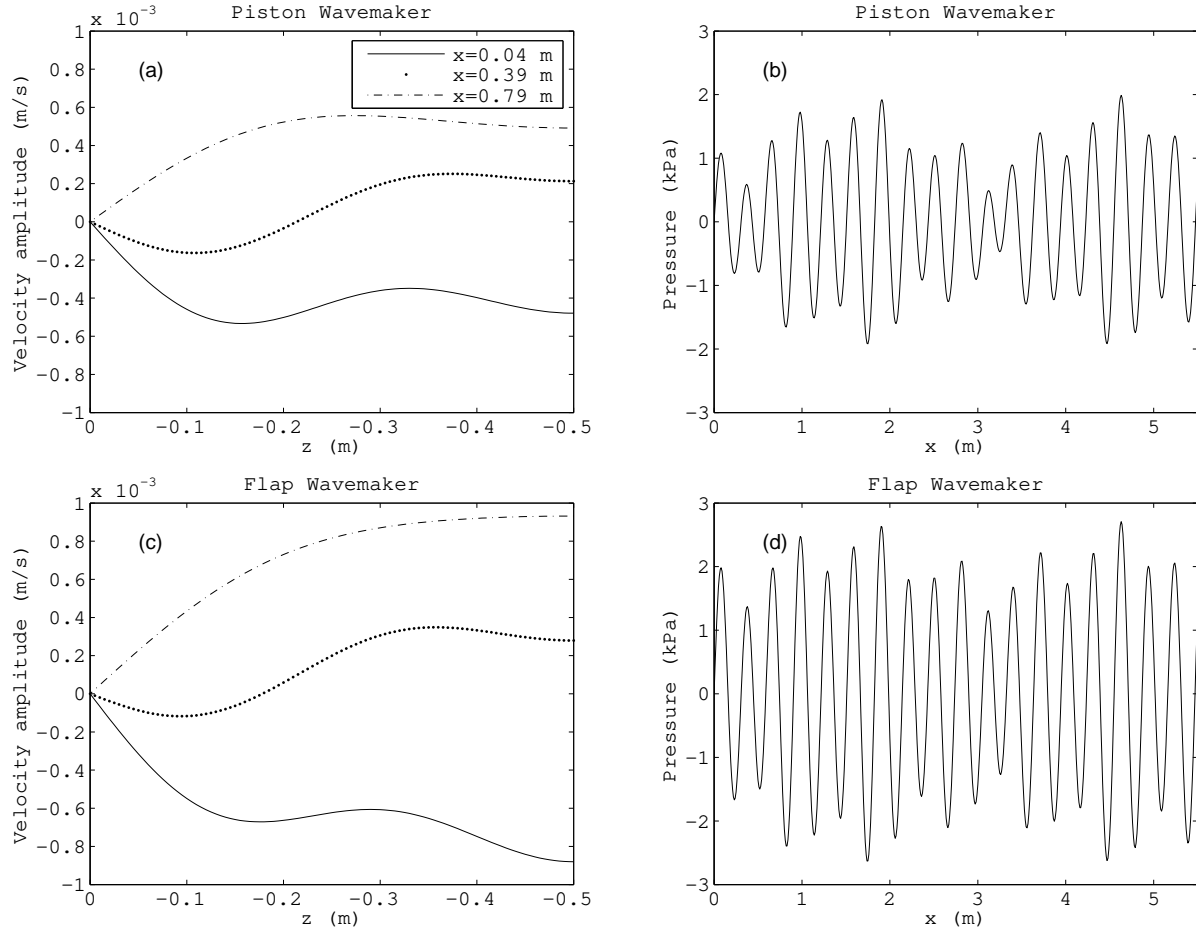


Figure 2: Acoustic-gravity waves generated by a wavemaker in a wave flume for  $f = 5$  kHz based on the Havelock's wavemaker theory;  $L = 5.5$  m,  $h = 0.5$  m,  $b = 1$  m,  $c = 1500$  m/s. The motion of the plate is limited by the constraint that, the horizontal movement  $\leq 2.1$  m, the horizontal velocity  $\leq 3.8$  m/s, horizontal acceleration  $\leq 19.6$  m/s<sup>2</sup> (parameters come from the unidirectional wavemaker in O.H. Hinsdale Wave Research Laboratory, Oregon State University). (a), (c) Vertical distribution of the velocity amplitude at  $x = 0.04$  m,  $0.39$  m, and  $0.79$  m away from the wavemaker. (b), (d) Horizontal distribution of the pressure amplitude at the bottom of the flume. (a), (b) piston wavemaker; (c), (d) flap wavemaker.

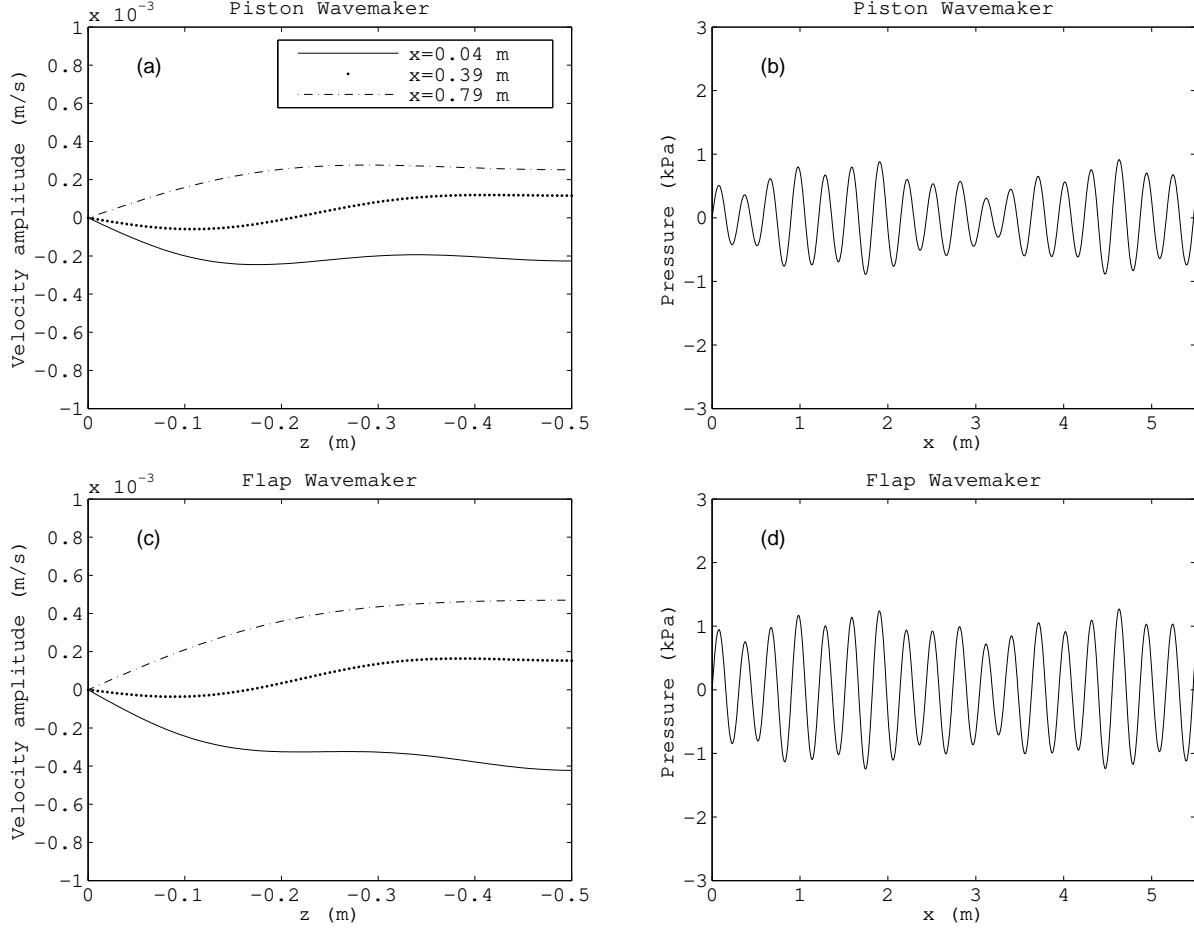


Figure 3: Acoustic-gravity waves generated by a wavemaker in a wave flume for  $f = 5$  kHz based on the porous wavemaker theory;  $L = 5.5$  m,  $h = 0.5$  m,  $b = 1$  m,  $c = 1500$  m/s. The motion of the plate is limited by the constraint that, the horizontal movement  $\leq 2.1$  m, the horizontal velocity  $\leq 3.8$  m/s, horizontal acceleration  $\leq 19.6$  m/s<sup>2</sup> (parameters come from the unidirectional wavemaker in O.H. Hinsdale Wave Research Laboratory, Oregon State University). (a), (c) Vertical distribution of the velocity amplitude at  $x = 0.04$  m,  $0.39$  m, and  $0.79$  m away from the wavemaker. (b), (d) Horizontal distribution of the pressure amplitude at the bottom of the flume. (a), (b) piston wavemaker; (c), (d) flap wavemaker.

## 5.2 Acoustic-gravity waves in deep ocean

We treat the problem of a wavemaker plate in deep ocean as a point source in deep water (similar to the ocean acoustics problem in Jensen et al. 2011), and consider it as a  $\delta$ -function. An example of a  $\delta$ -function wavemaker located at  $z = -12.5$  m in deep ocean with  $f = 1$  Hz and  $h = 4000$  m is presented in Figure 4 for both Havelock's and porous wavemaker theories. The AGWs produced by an impermeable wavemaker ( $G = 0$ ) have larger amplitudes (Figure 4 (a) and (b)), whereas the wave amplitude decreases as the wavemaker becomes porous ( $G \neq 0$ ). The surface elevation increases to  $10^{-3}$  m (not shown) compared to those in the laboratory example, although still hard to be distinguished from that of surface gravity waves. The velocity amplitudes are almost zero at the

surface; they reach their maximum at about  $z = 500$  m, and oscillate across the water column in the  $z$ -direction. Although AGWs have similar frequencies as the gravity mode, their distributions are periodic throughout the water column (i.e. do not decay with depth), therefore can be distinguished from the decaying behavior of gravity waves. The order of magnitude of the velocity reaches  $10^{-2}$  m/s, which is measurable by standard instruments such as the ADCP (Acoustic Doppler Current Profiler), PCADP (Pulse-coherent Acoustic Doppler Profiler). It is thus suggested to make use of pressure sensors at the seabed, or deep below the surface, where surface-wave signatures are negligible. The AGWs signal, however, is at the order of 10 kPa, which is easy to measure (e.g., the MODE experiment that measures the pressure fluctuation on the deep-sea floor by Brown et al., 1975). This simple example shows that AGWs may be responsible for the low-frequency oceanic noise on the seabed (e.g., Ardhuin et al., 2013).

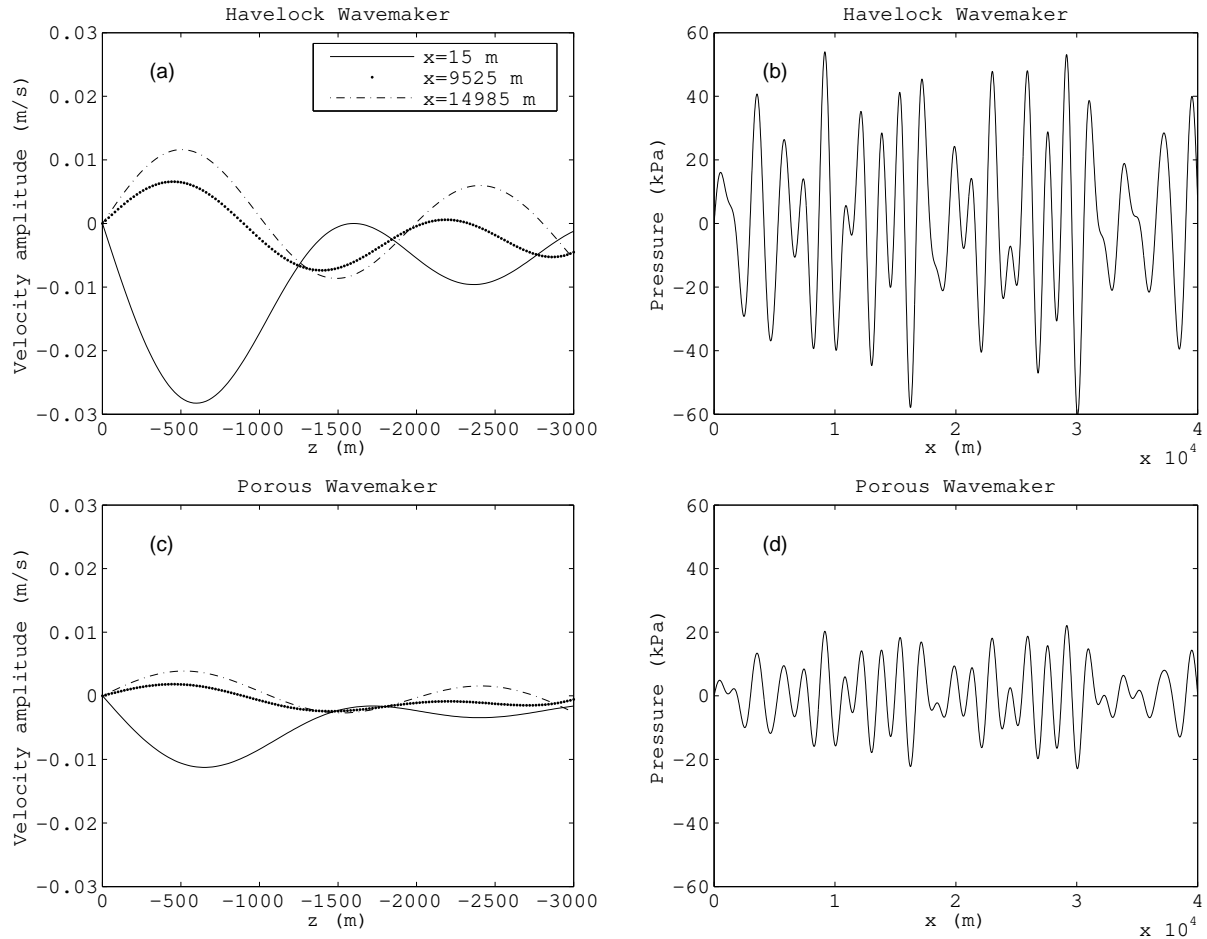


Figure 4: Acoustic-gravity waves generated by a  $\delta$ -function wavemaker in the ocean placed at  $z = -12.5$  m for  $f = 1$  Hz. The ocean is  $h = 4000$  m deep and the speed of sound is  $c = 1500$  m/s. (a), (c) Vertical distribution of the velocity amplitude at  $x = 15$  m, 9525 m, and 14985 m away from the wavemaker. (b), (d) Horizontal distribution of the pressure amplitude at the bottom of the flume. (a), (b) Havelock's wavemaker theory; (c), (d) porous wavemaker theory.

## 6 Conclusion

Without the usual overlook of the slight compressibility of water, we present Havelock's and porous wavemaker theories to analyze different modes of water waves following Dean and Dalrymple (1991) and Chwang (1983), with special focus on understanding the AGW mode. These theories may have important implications in the study of surface waves in flume experiment (Stuhlmeier and Stiassnie, 2015) or tsunamis caused by landslides during earthquakes in deep ocean (Yamamoto, 1982; Stiassnie, 2010; Kadri and Stiassnie, 2012). Moreover, the generation of acoustic-gravity waves can be attributed to wave-structure interaction (Stuhlmeier and Stiassnie, 2015), therefore another possible implication is where the efficiency of wave-energy harnessing devices is of interest, with the wavemaker being subjected to some form of wave energy converter, e.g., a flap gate (e.g., Sammarco et al., 2013). Another and probably a more immediate implication is the remote detection of the wavy sea-state which can help tuning the surface wave energy converters for maximum efficiency. These are left for future study, and we hope this work will motivate scientists and engineers to look into these important implications.

Both Havelock's and porous wavemaker solutions reduce to previous theories (Dean and Dalrymple, 1991; Chwang, 1983) for incompressible flow when the compressibility coefficient  $k_c$  in equation (13) tends to zero. The solutions for three types of plates as well as the spatial distribution of the AGWs components are presented. Having the same horizontal displacements of the plate, the results suggest that a flap wavemaker is capable of making larger waves than piston and  $\delta$ -function-type wavemakers. The spatial distribution of the amplitude of the surface elevation, horizontal velocity, and bottom pressure due to both theories was compared. It is shown that, generally, the porous wavemaker results in smaller waves than those produced by Havelock's theory due to the porosity factor  $G_n$  in equation (29). The calculations reveal that the surface elevation of AGWs in the current lab experimental settings is at the order of  $10^{-9}$  m, and can reach  $10^{-3}$  m in deep ocean. Therefore surface elevation of AGWs is hard to measure; while velocity amplitude suggests that AGWs can be detected by a particle image velocimetry (PIV) system in the laboratory experiment. Finally, the pressure distributions show that AGW signals are significantly large at the bottom of a wave flume and deep ocean, to be captured by a standard pressure sensor. This study motivates further laboratory studies and field measurement on deep ocean as it predicts the characteristics of these waves, thus provides insights on how to carry out direct measurements. It also sheds some light on development of tsunami early-detection systems from the perspective of describing AGWs near the epicenter when earthquakes occur. Finally, the porous wavemaker theory can potentially contribute to the study of deep-ocean energy-harvest device where the porous plates can be treated as an energy absorber.

## Acknowledgment

The first author acknowledges the Postdoctoral Fellowship at the University of Haifa in collaboration with Woods Hole Oceanographic Institution, part of which this work took place.

## References

- Ardhuin, F., Lavanant, T., Obrebski, M., Marié, L., Royer, J.-Y., D'Eu, J.-F., Howe, B. M., Lukas, R. & Aucan, J. (2013) A numerical model for ocean ultra-low frequency noise: wave-generated acoustic-gravity and Rayleigh modes.. *J. Acoust. Soc. Am.*, 134(4), 3242–59.
- Brown W., W. Munk, F. Snodgrass, H. Mofjeld and B. Zetler (1975), MODE bottom experiment. *Journal of Physical Oceanography*, 5, 75-85.
- Chwang, A.T. (1983) A porous-wavemaker theory. *Journal of Fluid Mechanics*, 132, 395- 406.
- Dalrymple R.A. (1989) Directional wavemaker theory with sidewall reflection, *Journal of Hydraulic Research*, 27:1, 23-34, DOI: 10.1080/00221688909499241.
- Dean R.G. and R.A. Dalrymple (1991), *Water Wave Mechanics for Engineers and Scientists*, Advanced Series on Ocean Engineering, Volume 2, 174, World Scientific, page 176.
- Eyov, E., Klar, A., Kadri, U., and Stiassnie, M. (2013), Progressive waves in a compressible ocean with elastic bottom, *Wave Motion* 50, 929-939. doi: 10.1016/j.wavemoti.2013.03.003
- Havelock, T. (1929) Forced surface-waves on water. *The London, Edinburgh, and Dublin Philosophical Magazine and Journal of Science*, 8(51), 569–576.
- Hendin G. and Stiassnie M. (2013) Tsunami and acoustic-gravity waves in water of constant depth, *Phys. Fluids* 25, 086103, doi: 10.1063/1.481799.
- Jensen, F.B., Kuperman, W.A., Porter, M.B., and Schmidt, H. (2011), *Computational Ocean Acoustics*, Modern Acoustics and Signal Processing, ISBN 978-1-4419-8678-8, Springer.
- Kadri, U. and M. Stiassnie (2012), Acoustic-gravity waves interacting with the shelf break. *Journal of Geophysical Research*, 117(C3), C03035.
- Kadri U. and M. Stiassnie (2013), Generation of an acoustic-gravity wave by two gravity waves, and their subsequent mutual interaction, *Journal of Fluid Mechanics*, 735, R61–R69.
- Kadri, U. (2014), Deep ocean water transport by acoustic-gravity waves. *Journal of Geophysical Research: Oceans*, 119(11), 7925–7930.
- Kadri, U. (2015) Wave motion in a heavy compressible fluid: Revisited, *Eur J Mech B-Fluid*, 49(A), 50-57.
- Kadri, U. (2016) Triad resonance between a surface gravity wave and two high frequency hydro-acoustic waves, *Eur J Mech B-Fluid* 55, 1: 157–161.
- Kadri, U. (2016) Generation of Hydroacoustic Waves by an Oscillating Ice Block in Arctic Zones, *Advances in Acoustics and Vibration*, 2016, 8076108, <http://dx.doi.org/10.1155/2016/8076108>
- Kadri, U. and Akylas, T.R. (2016) On resonant triad interactions of acoustic–gravity waves, *J. Fluid Mech* 788: R1(12 pages), doi:10.1017/jfm.2015.721.

- Lamb, H. (1916), *Hydrodynamics*, Cambridge: at the University Press, 4th edition, pp352.
- Madsen, O. S. (1970), Waves generated by a piston-type wavemaker. In *Proc. 12th Coastal Engng Conf.*, 589-607, ASCE.
- Mei C.C. (2012) Hydrodynamic principles of wave power extraction, *Phil. Trans. R. Soc. A* 370 , 208–234 doi:10.1098/rsta.2011.0178.
- Oliveira, T. C. A. and Kadri, U. (2016), Pressure field induced in the water column by acoustic-gravity waves generated from sea bottom motion. *J. Geophys. Res. Oceans*. Accepted Author Manuscript. doi:10.1002/2016JC011742
- Sammarco P., S. Michele, M. d’Errico (2013), Flap gate farm: From Venice lagoon defense to resonating wave energy production. Part 1: Natural modes, *Applied Ocean Research*, 43, 206–213.
- Stiassnie, M. (2010), Tsunamis and acoustic-gravity waves from underwater earthquakes, *J. Eng. Math.*, 67, 23–32, doi:10.1007/s10665-009-9323-x.
- Stuhlmeier, R., M. Stiassnie, Adapting Havelock’s wave-maker theorem to acoustic-gravity waves, *IMA J. Appl. Math.*, (accepted).
- Taylor, G.I. (1956) Fluid flow in regions bounded by porous surfaces. *Proc. R. Soc. Lond.* A234, 45-75.
- Tian M., Sheremet A., Kaihatu J.M., Ma G-F (2015) On the Shoaling of Solitary Waves in the Presence of Short Random Waves, *Journal of Physical Oceanography*, Vol. 45, No. 3, pages 792-806.
- Ursell, F., R.G. Dean, and Y.S. Yu (1960) Forced small-amplitude water waves: a comparison of theory and experiment. *J. Fluid Mech.* 7, 33-52.
- Yamamoto, T. (1982), Gravity waves and acoustic waves generated by sub- marine earthquakes, *Soil Dyn. Earthquake Eng.*, 1, 75–82.